Supporting Information

Engineering surface exposed $LaCoO_3$ perovskite nanotubular catalyst for catalytic combustion of toluene through acid etching

Shixing Wu[a, b#], Zhan Shi[a, e#], Fang Dong[a], Xin Song[c], Weiliang Han[a, c*], Weigao Han[a], Haitao Zhang[d], Xiuyan Dong[e], Zhicheng Tang[a, c*]

([a] National Engineering Research Center for Fine Petrochemical Intermediates, State Key Laboratory for Oxo Synthesis and Selective Oxidation, Lanzhou Institute of Chemical Physics, Chinese Academy of Sciences, Lanzhou 730000, China.

[b] University of Chinese Academy of Sciences, Beijing 100039, China.

[c] Shandong Laboratory of Advanced Materials and Green Manufacturing at Yantai, Yantai Zhongke Research Institute of Advanced Materials and Green Chemical Engineering, Yantai 264006, China.

[d] Lanzhou Petrochemical Research Center, Petrochemical Research Institute, PetroChina, Lanzhou 730060, China.

[e] School of Chemistry and Chemical Engineering, Lanzhou Jiaotong University, Lanzhou 730070, China.)

[#]These authors contributed equally: Shixing Wu, Zhan Shi.

---

*Corresponding author.

E-mail address: tangzhicheng@licp.cas.cn (Z. Tang), weilianghan@licp.cas.cn (W. Han).

1. Catalyst characterizations

The morphology of the catalyst samples was analyzed by transmission electron microscopy (TEM, JEOL-JEM-2010). Scanning electron microscope (SEM) images of the samples were obtained by a JSM-6701F cold field emission scanning electron microscope. The crystal phases of each element in the catalyst were determined by an X-ray diffraction instrument (XRD, Japan Smartlabse) (scanning angle of 10°-90°, scanning speed of 0.5 °/min, 60 kV, 55 mA) under the radiation of λ=1.5406 nm. The Fourier transform infrared spectroscopy (FTIR) analysis of the samples was performed using a Fourier infrared spectrometer (Nexus 870, Nicolet), and ATR technology was used for FTIR analysis. Brunauer-Emmett-Teller (BET) surface area, the pore size, and the pore volume of the catalysts were obtained by adsorption and desorption of nitrogen in the ASAP 2020 instrument (America Micromeritics). The real content of each metal on the catalyst was obtained by measuring each catalyst with an Agilent ICP-OES 730 instrument. Infrared spectra were tested with a Nicolet Nexus 870 Fourier transform infrared spectrometer. X-ray photoelectron spectroscopy (XPS) measurements were performed with a Thermo Scientific 250 Xi.

The multifunctional dynamic adsorption instrument TP-5080-D was used to analyze the acidity and redox capacity of the catalyst surface. For H_2-TPR, a 50 mg sample was heated from room temperature to 900 ^oC in reduced gas with volume fractions of 5 vol % H_2 and 95 vol % N_2, and the detector signal was continuously recorded. For the O_2-TPD test, the catalyst (50 mg) was pretreated with nitrogen (99.9%) for 1 h at 300 ^oC. When the temperature dropped to 50 ^oC, the O_2 (5% O_2/N_2)

adsorption was carried out for 60 min. After the adsorption was over, purged for 0.5 h, and the desorbed O_2 signal was detected at 50-900 °C. The temperature-programmed desorption operation of NH_3-TPD and SO_2-TPD was similar to that of O_2-TPD, except that O_2 was changed to NH_3 and SO_2.

2. Catalytic activity measurements

The activity and stability of the catalysts were tested with the help of toluene (C_7H_8) as a probe molecule, which was essential for the study of the catalytic oxidation performance of VOCs. The catalytic oxidation of toluene was evaluated by using a fixed-bed flow reactor operating at steady-state flow mode. Then, 0.4 g catalysts (40-60 mesh) and 0.7 g quartz sand (40-60 mesh) were mixed uniformly. They were put onto the reactor. The reaction gas containing VOCs (3000 ppm) was generated by bubbling air through a VOC saturator, and then passed through the reactor with a weight hourly space velocity (WHSV) of 30000 ml g^{-1} h^{-1}. The first temperature was 100 °C. The activity was measured per 20 °C. Before each test, it needed to stabilize for 1 h. Reactants and products were analyzed with an online GC-6820 gas chromatograph with a flame ionization detector, Conversion was defined as. The conversion efficiency of C_7H_8 was calculated by the following equation:

$$x = \frac{C_{in} - C_{out}}{C_{in}} \times 100\%$$

Where x is the conversion of C_7H_8, C_{in} and C_{out} are the inlet and outlet concentrations of C_7H_8 in the gas phase.

3. In situ FTIR measurement

In situ diffuse reflectance infrared Fourier transform spectroscopy (DRIFTS) spectra were collected with VERTEX 70 spectrometer equipped with an MCT detector and a CaF_2 window in-situ cell. DRIFTS cell was used as the reaction chamber and the spectra were collected in the frequency range of 4000-600 cm^{-1}. 200 mg grain catalyst (40-60 mesh) was packed in the DRIFTS cell. For C_7H_8 adsorption spectra, the LCCO-2 catalysts were pretreated at 300 ^oC by flowing N_2 for 30 min. After the temperature cooled to 50 ^oC, it was exposed to 15 ppm C_7H_8/ N_2 feed at a flow rate of 25 mL/min, and the adsorption was saturated. Subsequently, the adsorption saturation was reached at different temperatures (50 ^oC,100 ^oC, 150 ^oC, 200 ^oC, 250 ^oC and 300 ^oC). For the oxidation of C_7H_8, the LCCO-2 catalyst was treated with air, and then the 15 ppm C_7H_8 in Ar was pre-adsorbed on the clean samples at 50 ^oC for 30 min. Subsequently, the air with a flow of 25 mL/min was poured and the in situ FTIR spectra were collected at different temperatures with a heating rate of 10 ^oC/min.

4. Kinetic studies

The catalytic performance could also be identified by kinetic studies, such as apparent activation energy (E_a), which was measured as follows:

$$\ln r = \frac{-E_a}{RT} + C \tag{1}$$

In equation (1), r represented the reaction rate ($mol \cdot s^{-1}$), T referred to the reaction temperatures, and C was a constant term.

$$r = \frac{F \times X_{toluene}}{W} \tag{2}$$

In equation (2), $X_{toluene}$ denoted the conversion of toluene, F indicated the feeding rate (mol·s^{-1}), and W corresponded to the mass of the catalyst. Therefore, the plots of lnr and 1000/T yielded the E_a value.

The kinetic studies also included specific reaction rates, such as the catalyst's mass (R_m), which was calculated required the following equation:

$$R_m = \frac{F \times \eta_{toluene}}{W} \tag{3}$$

$$\eta_{toluene} = \log \frac{1}{1 - \frac{X_{toluene}}{100}} \tag{4}$$

Turnover frequency (TOF), defined as the number of toluene molecules converted per active site per second, is calculated according to the equation:

$$\text{TOF} = \frac{F_{toluene} * X_{toluene}}{\frac{\left(x(Co^{3+}) * x(Co) + x(Ce^{3+}) * x(Ce)\right)}{M_{Cat}} * m_{Cat}} \tag{5}$$

Where $F_{toluene}$ is the propane flow rate (mol/s), $X_{toluene}$ is the conversion of toluene, m_{cat} is the mass of the catalyst (g), M_{Cat} (g) is the malar of the catalysts, $x(Co^{3+})$ are the ratios of Co^{3+}/Co_{total}, $x(Ce^{3+})$ are the ratios of Ce^{3+}/Ce_{total} respectively; x(Co) is the total contents of Co in various samples and x(Ce) is the total contents of Ce in various samples (obtained by XPS experiments).

5. Computational Method

The Dmol^3 program in the Material Studio 2017 software suite was used to complete all calculations [1]. The molecular geometry, including the anatase $LaCoO_3$ (110), $La_{0.9}Ce_{0.1}CoO_3$ (110) and $vLa_{0.9}Ce_{0.1}CoO_3$ (110) surface, C_7H_8, was optimized using the GGA/PBE approach with a DNP basis [2]. For the core electrons of H, C, and O, the all-electron method was implemented, whereas for La, Co and Ce, the density functional semi-core pseudopotential method was used. The spin-polarized set was employed for all calculations, and the Grimme method was used for DFT-D correction. The values of 1.0×10^{-6} hartree (Ha), 1.0×10^{-5} Ha, 2.0×10^{-3} Ha/Å, and 5.0×10^{-3} Å, respectively, were the tolerances for SCF, energy, gradient, and displacement convergence [3]. At the same theoretical level, the electronic energies and zero-point vibration energies (ZPVE) were estimated.

References

1. B. Delley, From molecules to solids with the DMol^3 approach, *J. Chem. Phys.*, 2000, **113**, 7756-7764.
2. J.P. Perdew, K. Burke and M. Ernzerhof, Generalized gradient approximation made simple, *Phys. Rev. Lett.*, 1996, **77**, 3865-3868.
3. T. Zhu, X. Song, T. Li, J. Hu, K. Qi, P. Gao, R. Cui and Z. Tang. Simultaneous catalytic removal of complex sulfur-containing VOCs over Mn-based hydrotalcite-like compounds: Active sites and oxidation mechanism. *Sep. Purif. Technol.*, 2024, **339**, 126694.
4. M. Wu, S. Ma, S. Chen and W. Xiang, Fe-O terminated $LaFeO_3$ perovskite oxide surface for low temperature toluene oxidation, *J. Clean. Prod.*, 2020, **277**, 123224.
5. Z. Sihaib, F. Puleo, G. Pantaleo, V. La Parola, J.L. Valverde, S. Gil, L.F. Liotta and A. Giroir-Fendler, The effect of citric acid concentration on the properties of $LaMnO_3$ as a catalyst for hydrocarbon oxidation, *Catal.*, 2019, **9**, 226.
6. H. Chen, G. Wei, X. Liang, P. Liu, H. He, Y. Xi and J. Zhu, The distinct effects of substitution and deposition of Ag in perovskite $LaCoO_3$ on the thermally catalytic oxidation of toluene, *Appl. Surf. Sci.*, 2019, **489**, 905–912.
7. C. Lv, J. Zhang, L. Yan, H. Chen and M. Hu, Boosting sulfur tolerance and catalytic performance in toluene combustion via enhanced-mechanism of Ce-Fe dopants incorporation of $LaCoO_3$ perovskite, *J. Environ. Chem. Eng.*, 2022, **10**, 108372.
8. Y. Li, S. Liu, K. Yin, D. Jia, Y. Sun, X. Zhang, J. Yan and L. Yang, Understanding

the mechanisms of catalytic enhancement of La-Sr-Co-Fe-O perovskite-type oxides for efficient toluene combustion, *J. Environ. Chem. Eng.*, 2023, **11**, 109050.

9. Z. Shi, F. Dong, W. Han, X. Dong and Z. Tang, Engineering Co_3O_4@3DOM $LaCoO_3$ multistage-pore nanoreactor with superior SO_2 resistance for toluene catalytic combustion, *Nanoscale*, 2024, **16**, 10760–10778.

Table S1

Comparison of catalysts reported in the literature for catalytic oxidation of toluene with this work.

Catalysts	T_{50} (^oC)	T_{90} (^oC)	Concentration (ppm)	GHSV mL $(g \cdot h)^{-1}$	Ref.
$LaFeO_3$	308	333	1000	20000	[4]
$LaMnO_3$	229	298	1000	60000	[5]
$LaCoO_3$	290	331	1000	30000	[6]
$La_{0.95}Ag_{0.05}CoO_3$	238	268	1000	30000	[6]
$La_{0.6}Ce_{0.4}Co_{0.6}Fe_{0.4}O_3$	190	318	1000	60000	[7]
$La_{0.5}Sr_{0.5}Co_{0.8}Fe_{0.2}O_{3-\delta}$	251	270	1000	30000	[8]
Co_3O_4@$LaCoO_3$	229	254	3000	30000	[9]
LCCO-2	203	241	3000	30000	This work
LCCO-4	211	253	3000	30000	This work

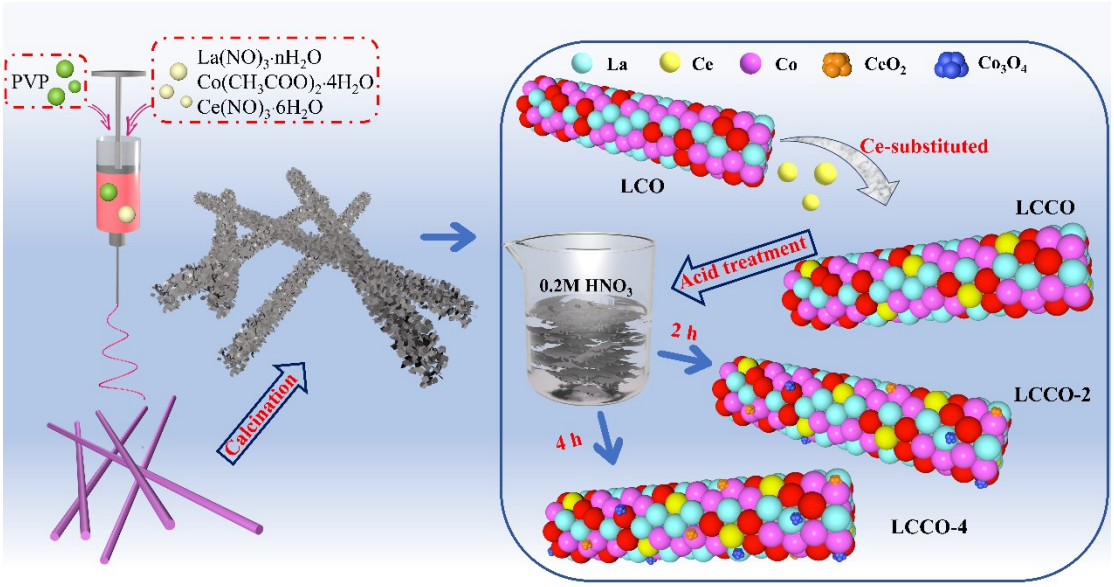

Fig. S1. Schematic diagram of the synthesis process for catalysts.

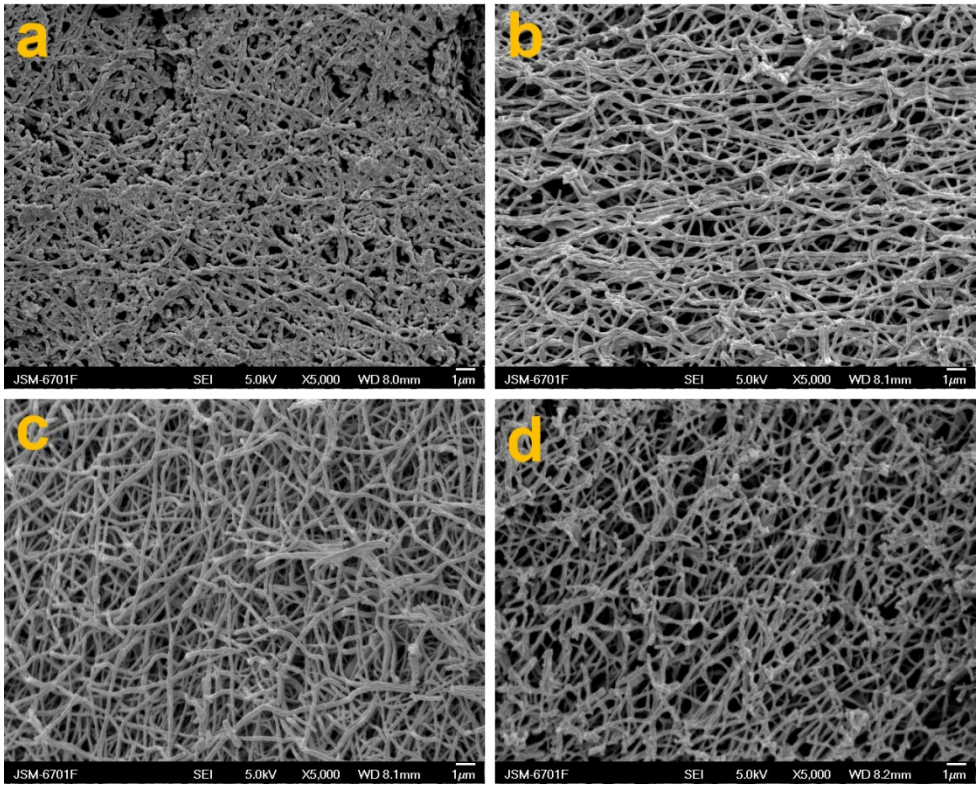

Fig. S2. SEM images of (a) LCO, (b) LCCO, (c) LCCO-2 and (d) LCCO-4 catalysts.

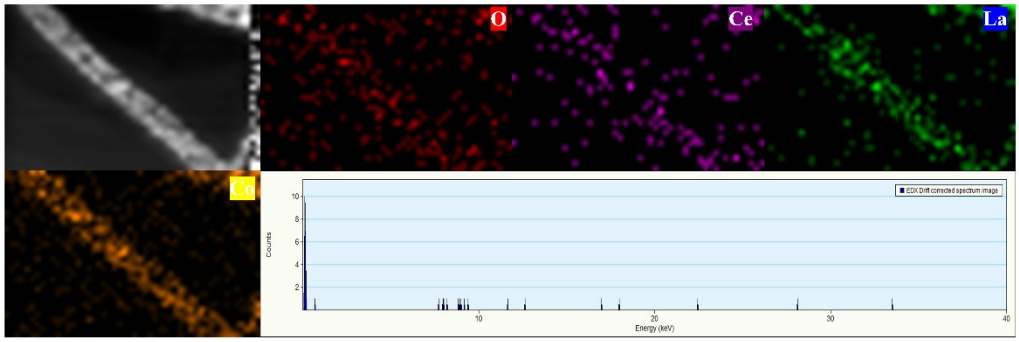

Fig. S3. Mapping analysis of LCCO catalyst.

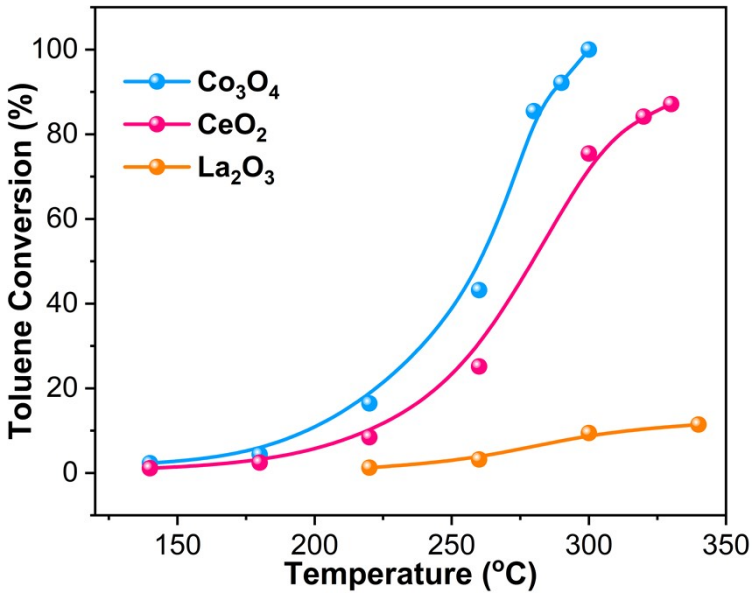

Fig. S4. Activity diagram of Co_3O_4, CeO_2 and La_2O_3 catalysts for the catalytic combustion of toluene.

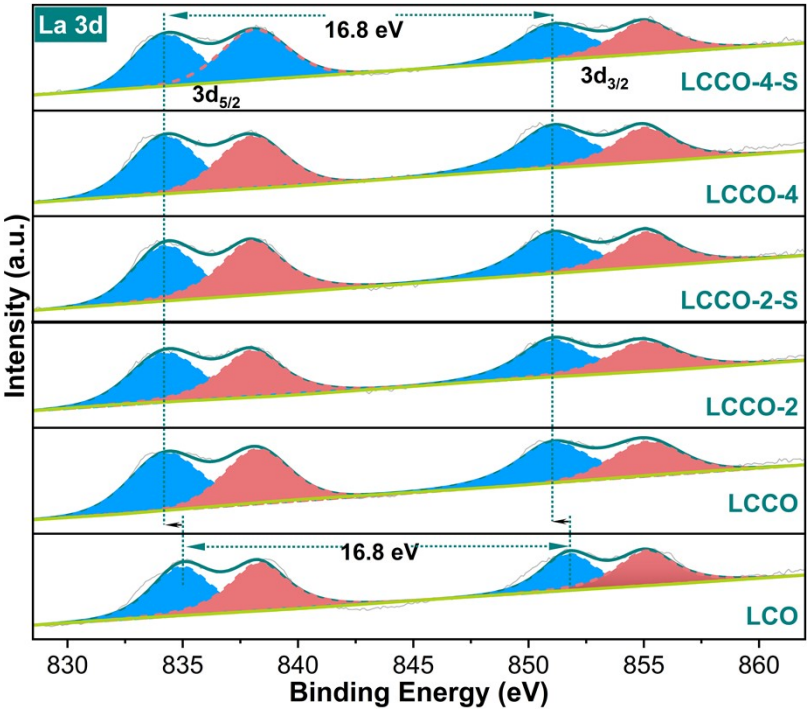

Fig. S5. XPS spectra of the La 3d on synthesized materials.

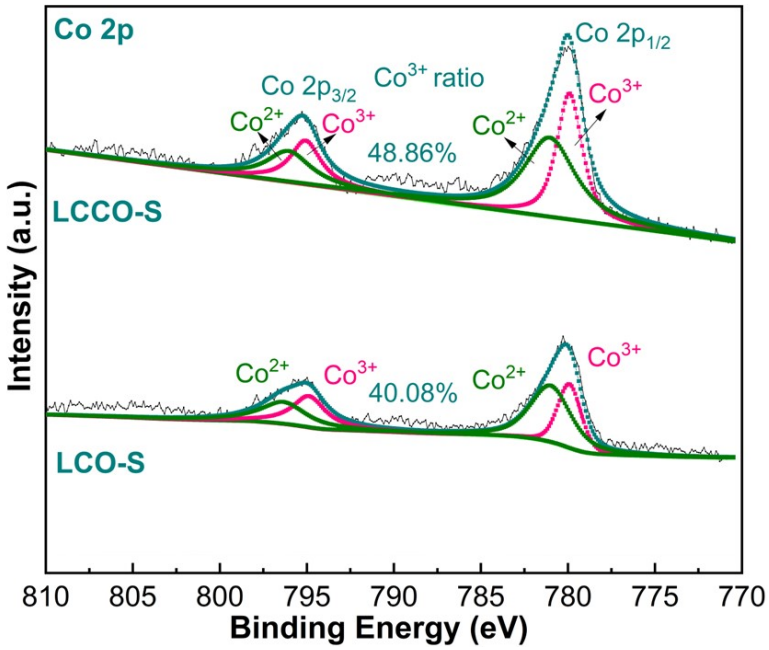

Fig. S6. XPS spectra of the Co 2p on LCO-S and LCCO-S materials.

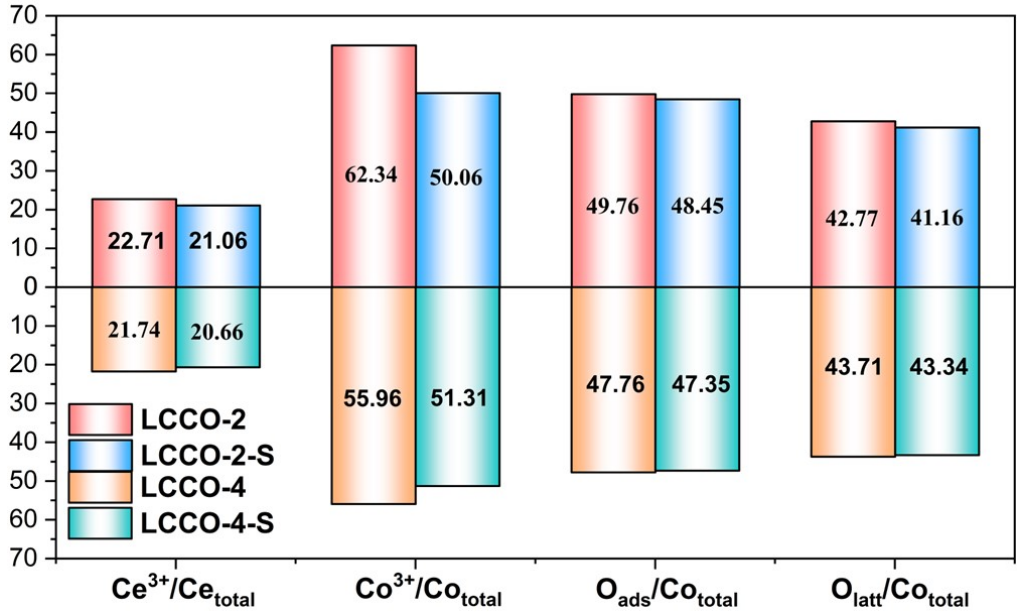

Fig. S7. Changes in Co^{3+}/Co_{total}, Ce^{3+}/Co_{total}, O_{ads}/O_{total}, O_{latt}/O_{total} after sulfur fluxing.

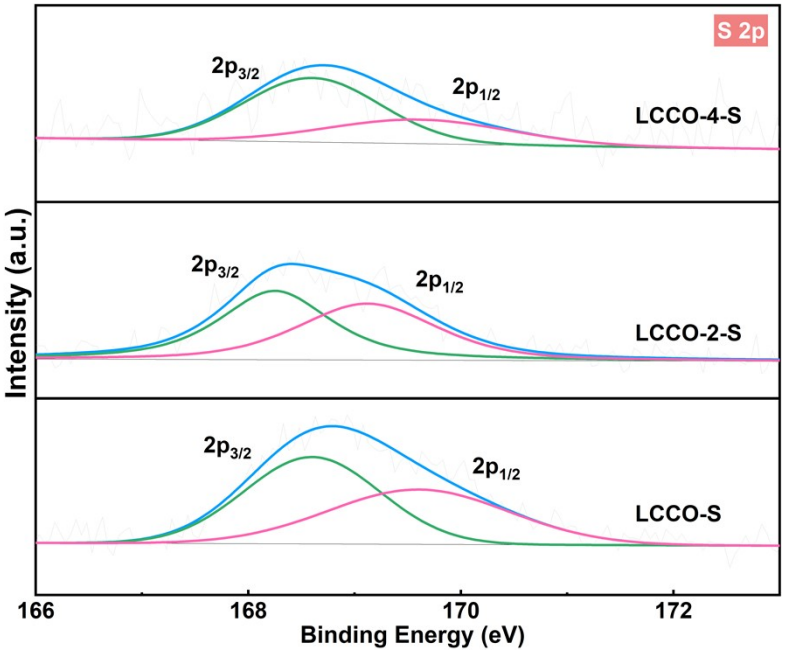

Fig. S8. XPS spectra of the S 2p on LCCO-S, LCCO-2-S and LCCO-4-S materials.

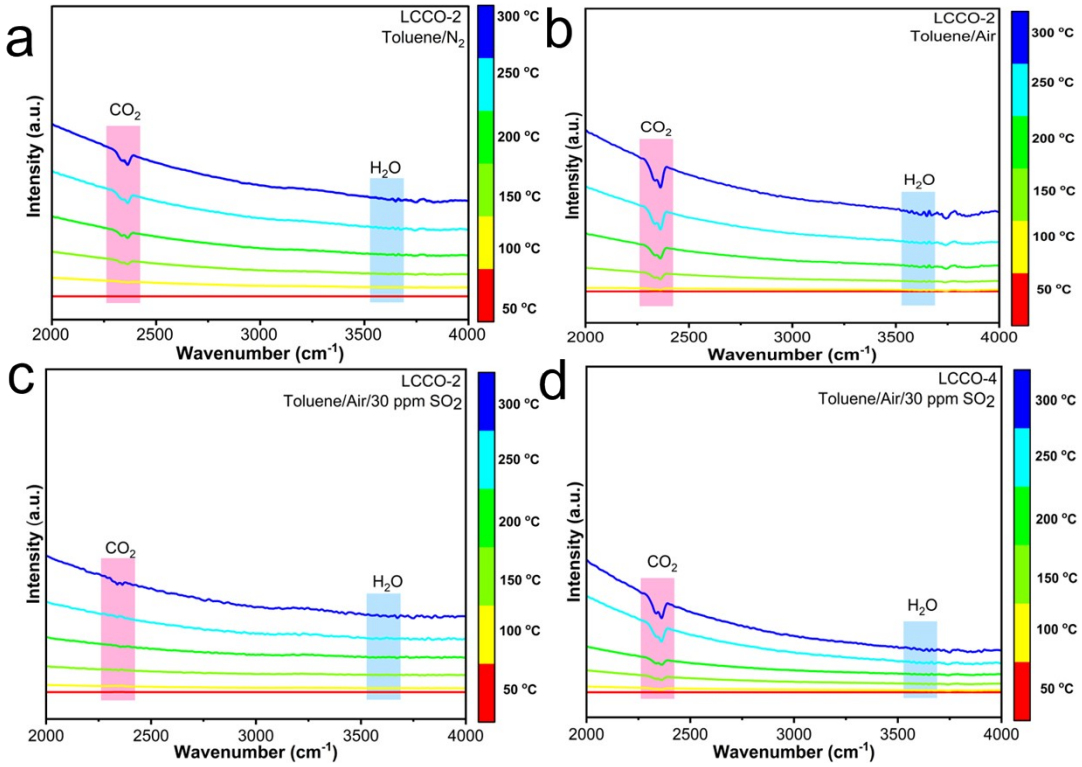

Fig. S9. In situ FTIR spectra of LCCO-2 catalyst exposed to (a) the flow of 15 ppm toluene and pure N_2 atmosphere, (b) the flow of 15 ppm toluene and air atmosphere, (c) the flow of 15 ppm toluene, 30 ppm SO_2 and 20% O_2/N_2 atmosphere; In situ FTIR spectra of LCCO-4 catalyst exposed to (d) the flow of 15 ppm toluene, 30 ppm SO_2 and 20% O_2/N_2 atmosphere.

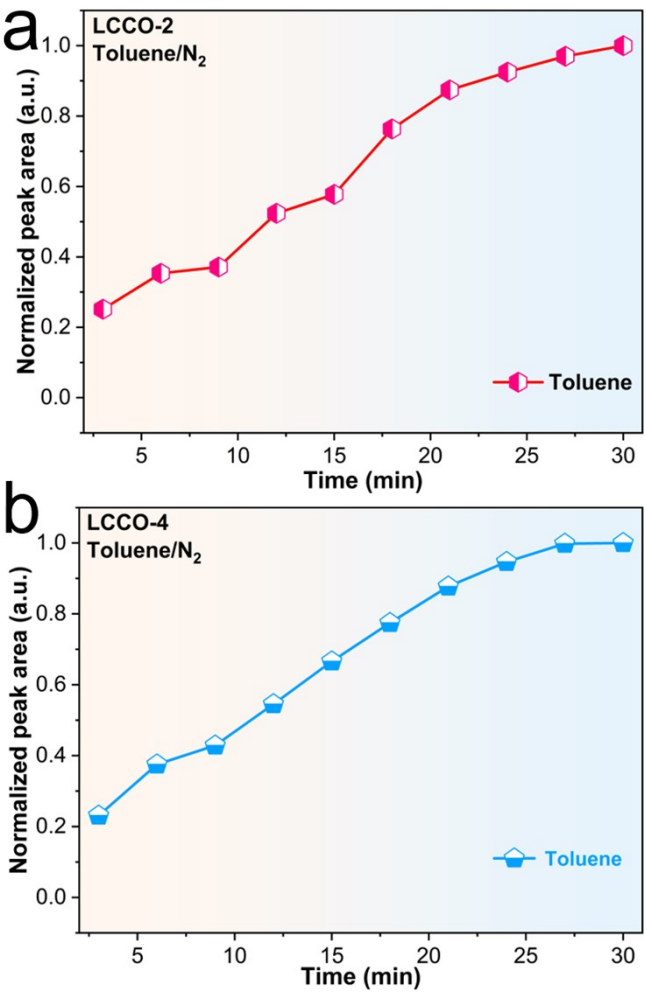

Fig. S10. The adsorption profiles of LCCO-2 and LCCO-4 catalysts exposed to 15 ppm toluene for different times.